Research on Chemical Intermediates
https://doi.org/10.1007/s11164-022-04824-4

Adsorption of iodine and reactive dye molecules from water using chemically modified and unmodified lignocellulosic powders (*Ficus Lyrata* seeds)

Oraphan Thongprasong[1] · **Haruthai Thananant**[1]

Received: 2 July 2022 / Accepted: 23 August 2022

Abstract

In this study, low-cost adsorbent was easily prepared from *Ficus lyrata* seed (FS) or lignocellulosic waste, and utilized for the efficient removals of iodine and reactive dye molecules. The lignocellulosic powder was easily treated using acid–base chemicals such as HNO_3 and KOH. The surface areas, porosities and morphologies of as-prepared adsorbent were analyzed by methylene blue adsorption method along with Langmuir calculation model. As obtained, rapid/multilayer-physisorption behaviors were interestingly found via Freundlich, Dubinin–Radushkevich, Temkin, pseudo-second-order and Weber–Morris models. The maximum capacities for iodine and reactive blue 19 molecules were found to be 340.00 (FS-Untreated) and 13.08 (FS-Treated by HNO_3) mg/g, respectively. The highest percentage removals of selected reactive dyes from synthetic wastewater using FS-Treated by HNO_3 were 58.30, 31.47 and 18.91% for reactive blue 19, reactive yellow 3 and reactive red 22, respectively, while 87.30% of iodine was removed using FS-Untreated. The endothermic and spontaneous adsorption of iodine and selected reactive dye molecules were verified under thermodynamic process. This research systematically studied on adsorption behaviors of iodine and reactive dye molecules, and provided high possibility to be truly applied in practical process for wastewater treatment.

✉ Oraphan Thongprasong
oraphan.t@rsu.ac.th

✉ Haruthai Thananant
haruthai.t@rsu.ac.th

[1] Department of Chemistry, Faculty of Science, Rangsit University, Lak Hok 12000, Pathumthani, Thailand

Published online: 16 September 2022

Graphical abstract

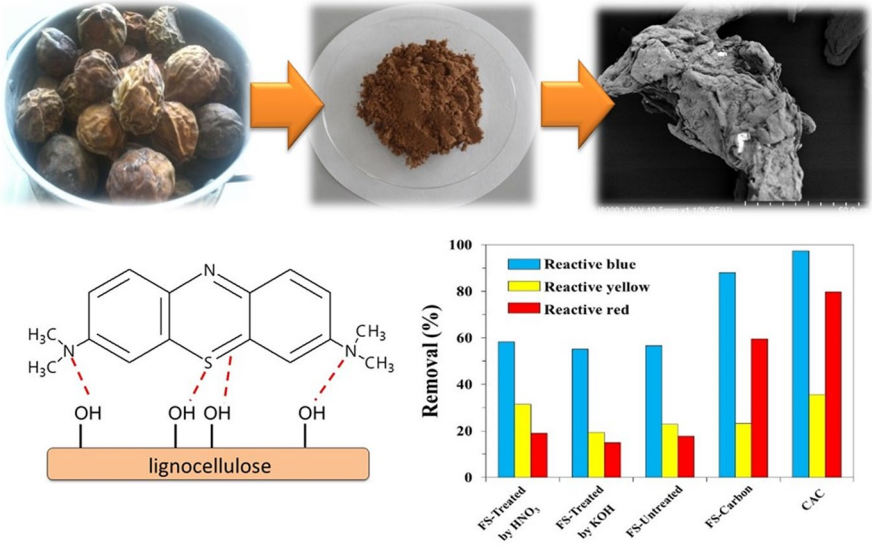

Keywords Lignocellulosic waste · Low-cost adsorbent · Iodine · Reactive dye · Adsorption

Introduction

Nowadays, the major problems in presence of toxic chemicals in environmental water should be considered since it is preliminary adulteration in worldwide [1]. The synthetic dyes are one of biggest group of water pollution, which highly discharged during printing, textile, cosmetics, food production processes. As reported, ~ 700,000 tons of organic dyes are generally produced in every year. Also, ~ 20% of dyes are released into natural water during manufacturing process. The presence of dye in natural water can generate many environmental problems; for instance, it can suppress oxygenation and photosynthetic activities of organisms [2, 3]. In the case of human health problems, it is toxic, mutagenic, teratogenic and carcinogenic [4]. Some types of reactive dyes can easily degrade and decompose to carcinogenic aromatic under aerobic/anaerobic conditions [5–9]. Likewise, iodine molecule is one of water pollution occurred from food, chemical and pharmaceutical processes [10]. Herein, it is also one section of nuclear fission by-product which is very high toxicity for human life. Therefore, it is necessary to find the green/facile way for efficient removal of dye and/or iodine [11, 12].

Many methods for removal/separation process have been intensively studied such as coagulation, flocculation, ion-exchange, precipitation, adsorption, ozonization and electrochemical photo-catalytic processes [13, 14]. Adsorption can be

considered as the most interesting method owing to low operating costs, non-complicated and environmental friendly processes [15]. In general, commercial activated carbon (CAC) is used as an industrial adsorbent for toxic adsorption/separation in wastewater [16, 17]. Shah et al. [18] found that the excellent removal of reactive orange 16 was achieved using phosphoric acid-activated carbon from Melia azedarach waste sawdust. Nevertheless, such kind of material is quite expensive and high C-footprint. Also, the production cost is high and complicate since pyrolysis system with the existence of N_2, He and steam is required to obtain high surface area and porosity of material. Thus, this is very important to find other materials in the present trend which can solve such above problems. Interestingly, lignocellulosic biomass is the most available material in the nature with the existence of high C content (> 60%) and excellent thermal stability. Here, there are attractive properties such as green/environmental friendly material, low-cost and high availability. Several lignocellulosic wastes such as rice husk, wood chip, sugarcane bagasse and other have been utilized for toxic removal in environmental wastewater [19–22]. Haroon et al. [23] succeeded on application of lignocellulosic wastes for Cr(VI) adsorption. To date, a few study on adsorption behaviors of iodine and reactive dye molecules has been performed over lignocellulosic wastes.

In this work, *Ficus lyrata* seed (FS) was applied as lignocellulosic adsorbent for the removal of iodine and reactive dye in aqueous solution. As known that iodine (non-polar molecule) can be easily adsorbed onto linkage of C–C bonds while the existence of –OH groups on lignocellulosic structure results in excellent ability for adsorption of reactive dye (polar molecule). The chemical structures of reactive blue 19, reactive yellow 3 and reactive red 22 applied for this study are shown in Fig. 1. The functional groups of FS were also treated using HNO_3 and KOH solutions using soaking process. The surface area and morphology of adsorbent sample were characterized by Langmuir-methylene blue adsorption, Fourier transform infrared spectroscopy (FTIR) and scanning electron microscopy (SEM) techniques. The adsorption abilities of iodine and reaction dye were investigated via effects of adsorbent amount and/or dye concentration. The adsorption behaviors of iodine and reaction dye onto FS adsorbent were systematically studied via isotherm, kinetic, intra-particle diffusion models and surface chemistries. Here, the literature investigations found that the use of FS has not been explored as low-cost/green adsorbent in this field. Advantage of this adsorbent in comparison with other one is high availability with large amount at low-cost preparation cost. In addition, the direct utilization of lignocellulosic waste can exactly reduce the problem of solid waste. In the case of economic point, it can possibly compete with CAC since it can easily prepare without energy consumption by pyrolysis process. Also, low-cost biomass presents the economic benefits for biosorption processes [24]. To the best of our knowledge, the utilization of FS adsorbent for adsorptions of iodine and reactive dye has not yet reported so far. This research is expected that the FS can be further applied as a green/low-cost adsorbent for toxic removal in industrial wastewater.

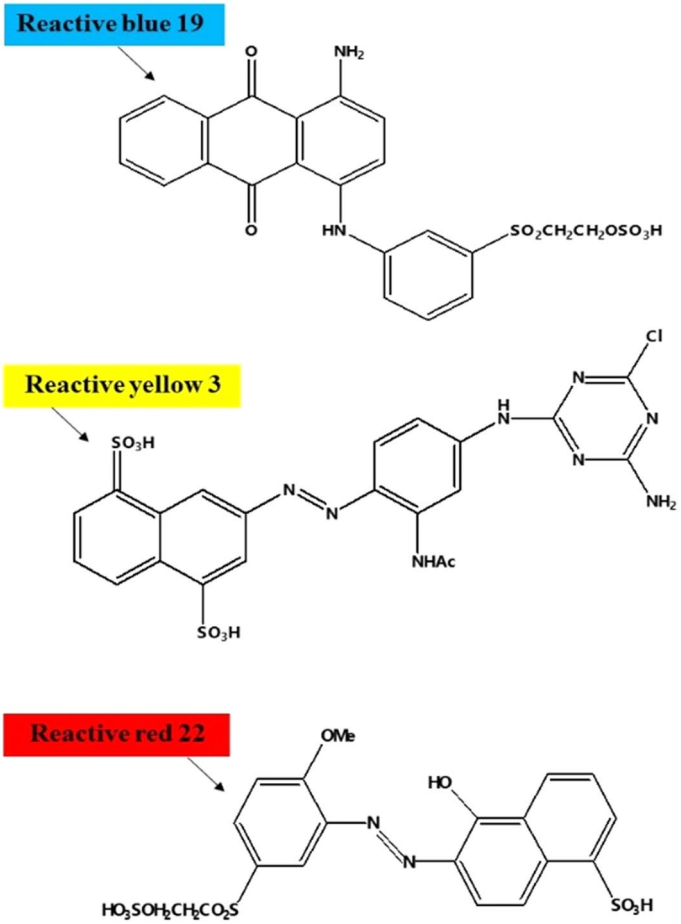

Fig. 1 Chemical structures of reactive blue 19, reactive yellow 3 and reactive red 22

Experimental

Stock solutions

Three kinds of reactive dyes such as reactive blue 19 ($Mw = 502$ g/mol and $\lambda_{max} = 580$ nm), reactive yellow 3 ($Mw = 608.5$ g/mol and $\lambda_{max} = 422.5$ nm) and reactive red 22 ($Mw = 514$ g/mol and $\lambda_{max} = 490.5$ nm) were applied as the pollution dye. The stock solutions such as reactive dye and iodine were prepared via dissolving in deionized water at initial concentrations of 100 mg/L and 0.2 mol/L, respectively.

Preparation of FS adsorbent

Ficus lyrata seed (FS) material was picked from Rangsit University, Pathumthani, Thailand, and utilized as a low-cost adsorbent. FS will be mashed via ball milling process and followed by sieving at 50 mesh. Finally, FS powder with a particle size around 297 µn was dried at 100 °C for overnight. The FS properties such as moisture, volatile matter, ash and fixed carbon were determined via proximate analysis using ASTM (D2866-94 and D2867-95) methods. Table 1 presents the proximate results of FS powder. Herein, the total percent of volatile matter + fixed carbon was obtained up to 75%, indicating that high C content was existed in FS structure.

For treatment process, 10 g of FS powder was mixed with 50 mL of 10%HNO_3 solution and then soaked at room temperature for overnight. Thereafter, FS-treated by HNO_3 was filtrated, washed with deionized water for several times and dried at 100 °C for overnight. In the case of KOH treatment, the preparation method, the amount and concentration of chemicals are the same with HNO_3 treatment process. Finally, the adsorbent samples were kept in desiccator before application for removals of iodine and reactive dye in aqueous solution.

Adsorbent characterization

The morphology of adsorbent was observed using a scanning electron microscope (SEM, JSM-5410 LV). The functional groups on FS were verified by Fourier transform infrared spectrometry (FTIR) using a PerkinElmer Spectrum 100 FTIR spectrometer. The FTIR results and discussion of FS before and after adsorption are provided in supporting information (SI) (Fig. S1) [13]. The surface area properties of adsorbent were investigated via methylene blue adsorption using Langmuir isotherm model with a maximum ability of monolayer adsorption. An adsorption interaction between methylene blue and biomass is shown in Fig. 2. The specific surface area can be calculated by following Eq. (1):

$$S = \frac{Q_0 \times N \times a_{MB}}{n} \tag{1}$$

where S is the specific surface area (m^2/g), Q_0 is the maximum monolayer adsorption capacity (mol/g), N is the Avogadro's number (6.02×10^{23} mol^{-1}), a_{MB} is the occupied surface area of one molecule of methylene blue (197.2 $Å^2$) and n is the amount of aggregation of methylene blue ($n = 2.5$).

Table 1 Proximate analysis of Ficus lyrata powder

Adsorbent	Proximate analysis (wt.%)			
	Moisture	Volatile matter	Ash	Fixed carbon[a]
Ficus lyrata powder	22.59	65.96	0.93	10.52

[a]Mass difference

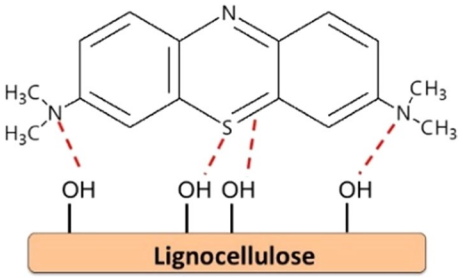

Fig. 2 Adsorption interaction between methylene blue and lignocellulosic surface

Adsorption procedure

The adsorption process was studied using a batch experiment. Herein, all samples were preliminary studied to find the optimal conditions for adsorption of iodine and selected reactive dyes before further investigations on isotherm and kinetic adsorptions with intra-particle diffusion. For adsorption procedure of iodine, 0.5 g adsorbent sample was mixed into 25 mL of iodine solution at concentration 0.1 N and stirred at a speed of 150 rpm with a room temperature for 30 min. After finishing process, the mixture solution was filtrated and analyzed to find the remaining concentrations of iodine. The amount of iodine was quantified by titration with thiosulfate standard solution. In the case of reactive dye (reactive blue 19, molecular weight = 502 g/mol) adsorption procedure, it was carried out at dye concentration of 5 mg/L under the similar conditions such the iodine adsorption process. After finishing adsorption of reactive blue dye, their remaining amount was determined by UV–Visible spectrophotometer at 580 nm (Genesys 20, USA). The adsorption capacity at equilibrium stage and the percentage removal of iodine and/or reactive dye were calculated by the following Eqs. (2) and (3), respectively:

$$q_e = (C_i - C_e)\frac{V}{M} \tag{2}$$

$$\text{Removal}(\%) = \frac{C_i - C_e}{C_i} \times 100 \tag{3}$$

where q_e is the adsorption capacity at equilibrium state (mg/g), C_i is the initial and equilibrium concentrations of iodine and/or reactive dye (mg/L), C_e is the concentrations of iodine and/or reactive dye at initial and equilibrium states (mg/L), V is the volume of iodine and/or reactive dye solution (L) and M is the mass of adsorbent (g). The results of each experiment were performed at least three-time tests to make sure all correction.

Results and discussion

Adsorption behaviors of iodine

Figure 3 presents effect of adsorbent amount for iodine removal. Here, the different amounts of samples from 0.25 to 2 g was carried out under iodine adsorption process. As expected, the removal percentages of iodine for all samples were increased to some extent with an increasing amount of adsorbent. This generally indicated that higher availabilities of adsorption site/surface were well occurred when more amount of adsorbent was applied [24]. However, too much amount of adsorbent adding might reduce the removal efficiency since aggregation phenomenon of adsorption site was promoted, resulting in a reduction of adsorption surface of adsorbent. Meanwhile, diffusion rate might be suppressed with the increasing of viscosity value in mixture system [13].

Figure 4 presents the treatment process of lignocellulosic biomass over acid–base chemicals. For acid treatment process, it could break down the rigid structure of lignocellulosic biomass via supporting by hydronium ions which could attack intermolecular bonds of cellulose, hemicellulose and/or lignin in lignocellulosic structure. Herein, it was interacted at β-1,4 glycosidic bonds in lignocellulosic structure [25]. In the case of alkaline/base treatment process, it is very specific for lignin structure in lignocellulose. The lignin structure could be easily destroyed via selective reaction of saponification at position of intermolecular ester bond via crosslink step between of xylan and lignin [26]. However, as presented in Fig. 3, the better ability for iodine removal was found in FS-Untreated while FS-Treated by HNO_3 was lower. It was possible that since polarity in FS structure was increased after treatment by

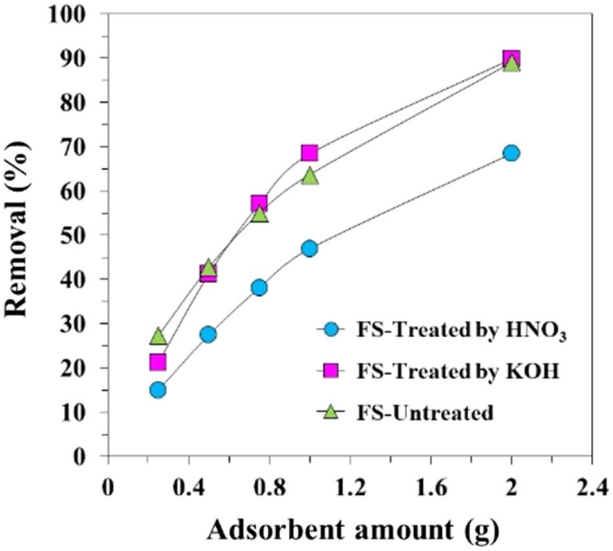

Fig. 3 Effect of amount of adsorbent on iodine removal efficiency using 25 mL of 0.1 N iodine concentration, 30 min of contract time and 0.25 to 2 g of adsorbents

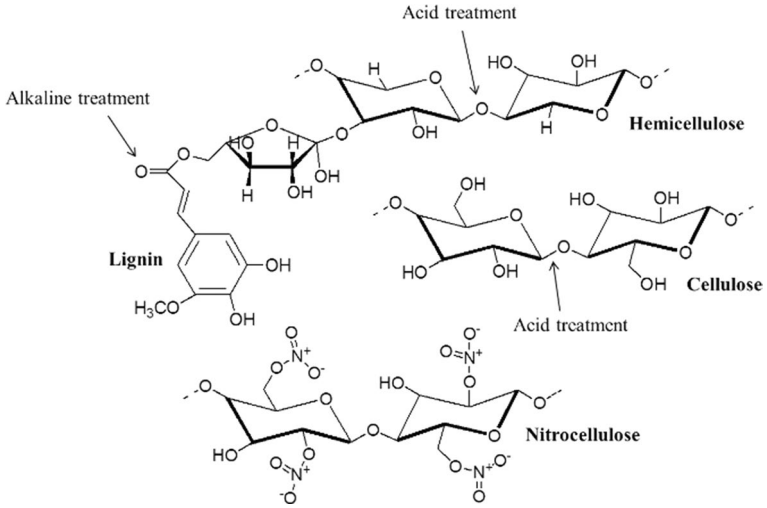

Fig. 4 Acid–base treatment of lignocellulosic biomass and formation of nitrate group on biomass structure

HNO_3, resulting in decreasing of adsorption ability of non-polarity molecule such iodine. As known that the main functional groups of FS structure were hydroxyl (OH-) and carbonyl (C=O) groups. After treatment by HNO_3, the esterification process was easily occurred between nitrate (NO_3^-) and hydroxyl groups to produce nitrocellulose, leading to formation of negatively charged surface in biomass structure (Fig. 4). Also, swelling of cellulose affected the increase in adsorption site [27]. Here, it could be further expected for improving the adsorption efficiency of reactive dye since it is polar molecule.

For equilibrium relationships between various adsorbents with iodine or reactive dye, four isotherm models were systematically applied to access the adsorption behaviors [28–31]. For (I) assumption of Langmuir model, the adsorption sites are uniformly distributed on the adsorbent surface, while the adsorbent and adsorbent had no interaction in each other, which was a monolayer adsorption. The nonlinear and linear models of Langmuir isotherm can be expressed by Eqs. (4) and (5), respectively:

$$q_e = Q_0 \frac{K_L C_e}{1 + K_L C_e} \tag{4}$$

$$\frac{C_e}{q_e} = \frac{1}{Q_0 K_L} + \frac{C_e}{Q_0} \tag{5}$$

where C_e is the adsorbate concentrations at equilibrium state (mg/L), q_e is the adsorption capacity at equilibrium state (mg/g), Q_0 is the maximum capacity for monolayer adsorption (mg/g) and K_L is the constant value of Langmuir model correlated to affinity of the binding sites and adsorption energy (L/mg).

For (II) assumption of Freundlich model, it could be described to non-homogeneously distributed on the adsorbent surface and the adsorbent and adsorbent belong to multilayer adsorption. The nonlinear and linear models of Freundlich isotherm can be expressed by Eqs. (6) and (7), respectively:

$$q_e = K_F C_e^{1/n} \tag{6}$$

$$\log q_e = \log K_F + \frac{1}{n}\log C_e \tag{7}$$

where K_F is the Freundlich constant correlated to the adsorption capacity [mg/g(L/mg)$^{1/n}$] and $1/n$ is the denseness of adsorption with constant value incorporating to some parameter, influencing the adsorption ability.

For (III) assumption of Temkin model, it could be described to interaction phenomena between adsorbent and adsorbate with heat value of adsorption. The nonlinear and linear models of Temkin isotherm can be expressed by Eqs. (8) and (9), respectively:

$$q_e = \left(\frac{RT}{b}\right)\ln(AC_e) \tag{8}$$

$$q_e = A + b \ln C_e \tag{9}$$

where A is the constant value at equilibrium stage correlated with a maximum binding energy (L/mol), R is the constant value of universal gas (8.314 J/molK^{-1}), T is the adsorption temperature (K) and b is the constant value of Temkin model correlated with an adsorption heat.

For (IV) assumption of Dubinin–Radushkevich model, it could be described to the free energy value with the adsorption porosity. The nonlinear and linear models of Dubinin–Radushkevich isotherm can be expressed by Eqs. (10) and (11), respectively:

$$q_e = q_s \exp(-B\varepsilon^2) \tag{10}$$

$$\ln q_e = \ln q_s - Be^2 \tag{11}$$

where q_s is the maximum capacity for theoretical adsorption (mg/g), B is the constant value of Dubinin–Radushkevich model correlated with an energy value from biosorption process (mol^2/kJ^2). Meanwhile, Polanyi potential value ($\mathcal{E}$) and free energy for adsorption process (E, kJ/mol) can be calculated by Eqs. (12) and (13), respectively:

$$\varepsilon = RTln\left(1 + \frac{1}{C_e}\right) \tag{12}$$

$$E = \frac{1}{\sqrt{2B}} \tag{13}$$

Herein, E value could be used to describe the adsorption behaviors; for instance, $E = < 8$ kJ/mol is physisorption process while chemisorption was in the range of ~ 8–16 kJ/mol.

Table 2 presents the isotherm results of iodine adsorption at equilibrium stage. It is found that Langmuir and Freundlich isotherms were well fitted for all samples based on R^2 value close to 1, indicating that the adsorption behavior of iodine was for multilayer + physisorption process. The maximum capacities of iodine adsorptions using FS-Treated by HNO_3, FS-Treated by KOH and FS-Untreated were found to be 124.54, 118.58 and 340.00 mg/g, respectively. It should be noted that higher adsorption ability was found in FS-untreated, indicating that the selective adsorption of non-polar molecule was preferred for FS without treatment process. Also, it is possible that adsorption behavior of iodine over FS-Untreated was for multilayer while FS-Treated by HNO_3, FS-Treated by KOH was more specific for monolayer adsorption. The constant values of $1/n$ for all samples were lower than 1, suggesting that multilayer adsorption behavior was favorable during the slight increments of q_e and C_e in adsorption system. For Temkin model, a maximum value of Temkin constant correlated with an adsorption heat was exhibited for FS-Untreated, resulting in excellent efficiency for natural removal of iodine. In the case of Dubinin–Radushkevich model, free energy values (E) for iodine adsorption process over various adsorbents were < 8 kJ/mol, indicating that adsorption behavior of iodine was physisorption process. These results were in well agreement with data of Langmuir and Freundlich isotherms.

Figure 5 presents the adsorption capacities of iodine at various contact times using FS-Treated by HNO_3, FS-Treated by KOH and FS-Untreated. One can see that the adsorption capacity was increased with the increase in contact times while the color of iodine solution was changed from brown to colorless for all samples. Only after 3 min, the iodine adsorptions for all samples were reached to the equilibrium state, suggesting to rapid adsorption behavior with the existence in large available of adsorption site. To obtain more details on adsorption behaviors, the adsorption kinetics of iodine were also studied via an adsorption dynamic in terms of adsorption rate constant [32, 33]. Here, pseudo-second order was described to rapid adsorption which could be generally occurred in non-porous materials or interaction between adsorbate with functional groups on adsorbent surface. In the case of pseudo-first order, it was occurred with slightly adsorption process via many steps of diffusion using porous materials. The nonlinear and linear kinetic models of pseudo-first order for adsorption mechanisms can be expressed by Eqs. (14) and (15), respectively:

$$q_t = q_e(1 - e^{-k_1 t}) \tag{14}$$

$$\log(q_e - q_t) = \log q_e - \frac{k_1}{2.303} t \tag{15}$$

Also, nonlinear and linear kinetic models of pseudo-second order for adsorption mechanisms can be expressed by Eqs. (16) and (17), respectively:

Table 2 Isotherm parameters on iodine and reactive blue 19 adsorptions over various adsorbents

Adsorbent	Iodine adsorption			Reactive blue 19 adsorption		
	Langmuir model			Langmuir model		
	Q_0 (mg/g)	K_L (L/mg)	R^2	Q_0 (mg/g)	K_L (L/mg)	R^2
FS-Treated by HNO_3	124.54	0.0003	0.9974	13.08	1.7025	0.9869
FS-Treated by KOH	118.58	0.0016	0.9988	12.47	1.3082	0.9825
FS-Untreated	340.00	0.0005	0.9062	12.59	1.4503	0.9847
Adsorbent	Freundlich model			Freundlich model		
	K_F	$1/n$	R^2	K_F	$1/n$	R^2
FS-Treated by HNO_3	0.7173	0.5558	0.9928	7.2073	0.4021	0.9886
FS-Treated by KOH	7.4611	0.3234	0.9803	6.1895	0.3843	0.9975
FS-Untreated	6.9762	0.4092	0.9776	6.4861	0.3883	0.9966
Adsorbent	Temkin model			Temkin model		
	b	A (L/mol)	R^2	b	A (L/mol)	R^2
FS-Treated by HNO_3	67.1823	1.0453	0.9845	3.9293	0.3743	0.9438
FS-Treated by KOH	35.4393	1.0195	0.9776	3.6022	0.3624	0.9617
FS-Untreated	98.3905	1.0108	0.8228	3.7011	0.3636	0.9694
Adsorbent	Dubinin–Radushkevich model			Dubinin–Radushkevich model		
	B (mol^2/J^2)	E (kJ/mol)	R^2	B (mol^2/J^2)	E (kJ/mol)	R^2
FS-Treated by HNO_3	2.28×10^{-1}	0.0021	0.9679	3.06×10^{-8}	5.7153	0.7967
FS-Treated by KOH	2.35×10^{-2}	0.0065	0.9370	3.67×10^{-8}	5.2215	0.7950
FS-Untreated	8.14×10^{-3}	0.0111	0.6450	3.55×10^{-8}	5.3042	0.8125

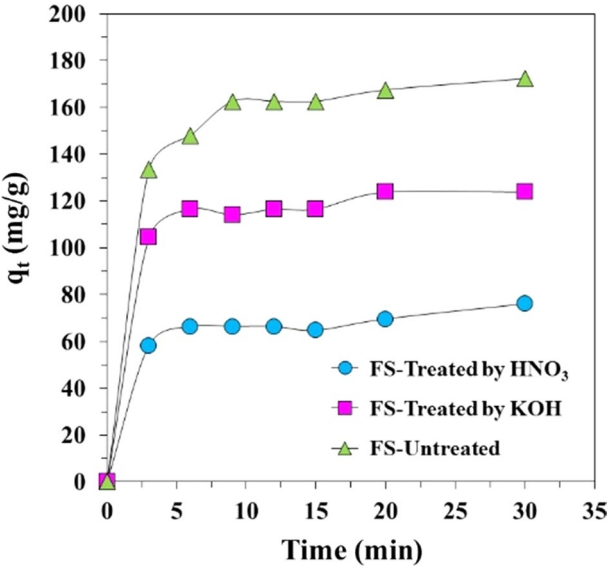

Fig. 5 Effect of contact time on iodine removal efficiency using 25 mL of 0.1 N iodine concentration, 3 to 30 min of contract times and 0.5 g of adsorbent

$$q_t = \frac{q_e^2 k_2 t}{1 + q_e k_2 t} \tag{16}$$

$$\frac{t}{q_t} = \frac{1}{k_2 q_e^2} + \frac{1}{q_e} t \tag{17}$$

where q_t (mg/g) is the adsorption capacity of adsorbate at various times. k_1 and k_2 values are the pseudo-first-order and the pseudo-second-order rate constants, respectively. t is the contact time of adsorption (min).

Table 3 presents the specific parameters obtained from kinetic models of iodine adsorption process. It is found that the adsorption kinetics of iodine using FS-Treated by HNO_3, FS-Treated by KOH and FS-Untreated were fitted with the characteristic of pseudo-second order (based on $R^2 > 0.99$), corresponding to rapid adsorption style. Herein, highest and lowest rate of iodine adsorption were in FS-Untreated (0.1237 min^{-1}) and FS-Treated by HNO_3 (0.0784 min^{-1}). Moreover, the kinetic models for iodine adsorption over as-prepared adsorbents presented well accuracy based on approximation of q_e value obtained from experiment and calculation procedures. To know more details on diffusion behaviors during iodine adsorption process, the effect of intra-particle diffusion was investigated via Weber–Morris model [34]. Figure 6 presents the intra-particle diffusion result of iodine onto as-prepared adsorbent. Normally, three stages for diffusion mechanisms were (I) in part of film layer and/or outer surface, (II) in part of pore layer and (III) in part of active/adsorption site. As obtained results, the curves of intra-particle diffusion of iodine on each sample exhibited two

Table 3 Pseudo-first-order and pseudo-second-order kinetic models and their parameters obtained the adsorptions of iodine and reactive blue 19 at different times over various adsorbents

Adsorbent	$q_{e,\exp}$ (mg/g)	Pseudo-first order			Pseudo-second order		
		$q_{e,\text{cal}}$	k_1	R^2	$q_{e,\text{cal}}$	k_2	R^2
Iodine adsorption							
FS-Treated by HNO_3	77.66	26.07	0.0784	0.8095	77.52	0.0080	0.9916
FS-Treated by KOH	131.06	24.66	0.0454	0.8040	126.58	0.0090	0.9989
FS-Untreated	182.02	43.19	0.1237	0.8678	178.57	0.0051	0.9996
Reactive blue 19 adsorption							
FS-Treated by HNO_3	0.38	0.02	0.0293	0.0525	0.38	3.3842	0.9933
FS-Treated by KOH	0.16	0.17	0.0962	0.9757	0.22	0.3636	0.9935
FS-Untreated	1.02	0.04	0.0930	0.1977	1.04	1.4668	0.9925

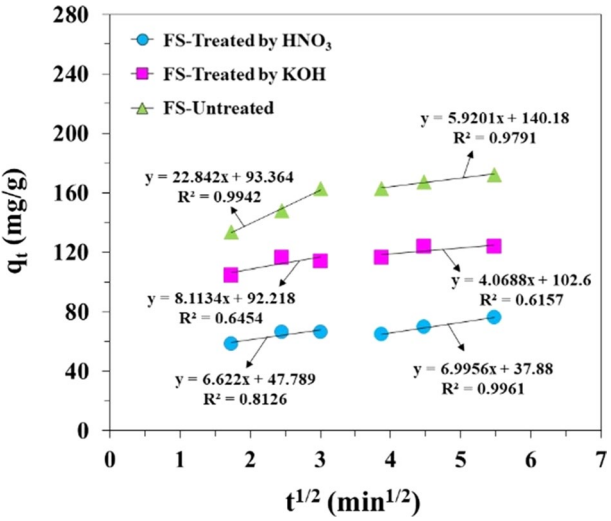

Fig. 6 Effect of intra-particle diffusion of iodine onto various adsorbents

regions which did not pass through the origin, suggesting that a rapid adsorption was well occurred via intra-particle diffusion with two-step.

For thermodynamic adsorption of iodine, it was analyzed at temperatures of 303–328 K, which standard enthalpy (ΔH), standard entropy (ΔS) and Gibbs standard free energy (ΔG) can be calculated by Eqs. (18–21):

$$K_d = \frac{C_0 - C_e}{C_e} \tag{18}$$

$$\Delta G = -RTlnK_d \tag{19}$$

$$\Delta G = \Delta H - T\Delta S \tag{20}$$

$$\ln K_d = \frac{\Delta S}{R} - \frac{\Delta H}{RT} \tag{21}$$

where T is the adsorption temperature (K) and K_d is the distribution coefficient.

Table 4 presents the specific parameters obtained from thermodynamic models of iodine adsorption process. The ΔG exhibited negative values and was in the range of −20 to 0 kJ/mol at all temperatures of 303–328 K, according to spontaneous physisorption of iodine using FS-Treated by HNO_3, FS-Treated by KOH and FS-Untreated [2]. Meanwhile, the increasing of adsorption temperature promoted the reduction of ΔG value, suggesting that iodine adsorption was endothermic trend. In addition, the positive values were found in results of ΔH and ΔS, which should be described to irreversible adsorption of iodine using all adsorbents [12].

Adsorption behaviors of reactive dye

Figure 7 shows the result of dye (reactive blue 19) removal at different concentration. One can see that a dramatic reduction in the removal efficiency of reactive dye was occurred for all samples when the initial concentration of dye was increased from 5 to 40 ppm. This phenomenon should be attributed to the fact that the total available adsorption sites were limited since adsorbent amount was fixed [35, 36]. Noticeably, the highest capacity for dye removal was found in FS-Treated by HNO_3, indicating that the FS treatment using HNO_3 was achieved for improving the adsorption efficiency of reactive dye. In the other words, the treatment by HNO_3 promoted the formation of nitrate and hydroxyl groups on FS structure which highly preferred for selective adsorption of polar molecule such a reactive dye. In addition, it might

Table 4 Thermodynamic parameters obtained the adsorptions of iodine and reactive blue 19 at different temperatures over various adsorbents

Adsorbent	ΔH (kJ/mol)	ΔS (J/mol.K)	ΔG (kJ/mol)				R^2
			303 K	313 K	323 K	328 K	
Iodine adsorption							
FS-Treated by HNO_3	12.78	42.38	−0.05	−0.48	−0.83	−1.01	0.9987
FS-Treated by KOH	11.79	41.15	−0.68	−1.01	−1.37	−1.56	0.9977
FS-Untreated	12.28	41.77	−0.36	−0.75	−1.10	−1.28	0.9999
Reactive blue 19 adsorption							
FS-Treated by HNO_3	15.82	62.08	−2.92	−3.42	−3.91	−4.09	0.9989
FS-Treated by KOH	27.93	94.11	−0.59	−1.42	−2.21	−2.71	0.9972
FS-Untreated	21.88	78.10	−1.76	−2.42	−3.06	−3.40	0.9994

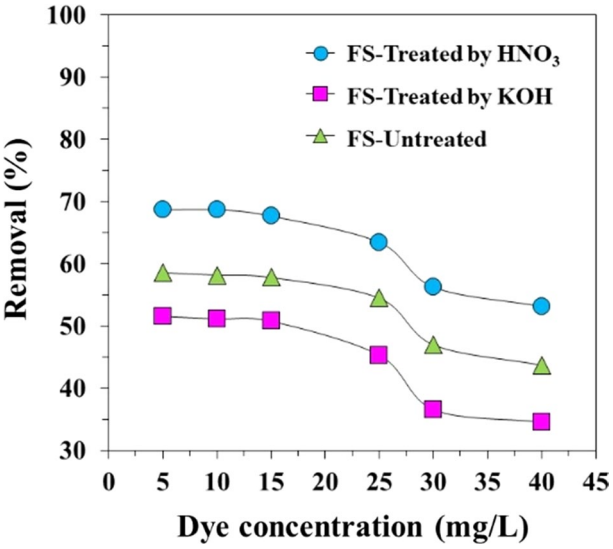

Fig. 7 Effect of dye concentration (reactive blue 19) on removal efficiency using 0.25 g of adsorbent, 30 min of contract time and 25 mL of dye with different concentration of 5–40 ppm

be described via theory of polarity with increasing on surface charge of FS after treatment by HNO_3. Unlikely, a lowest efficiency for dye removal was presented for FS-Treated by KOH, probably due to the facile destruction of FS by KOH via converting process of lignocellulose into salt.

Table 2 presents the isotherm data for dye (reactive blue 19) adsorption. As obtained, the adsorption behavior of reactive dye for all samples well exhibited the trend of multilayer style which supported by Freundlich model based on R^2 close to 1. This indicates that not only dipole–dipole force was occurred during dye adsorption process, but also the presence of mass attraction in each layer. The highest constants of Langmuir, Freundlich and Temkin isotherms were obtained for FS-Treated by HNO_3, resulting in high selectivity for dye adsorption. This could be confirmed that the adsorption process of reactive dye in this study was physisorption trend based on free energy values (<8 kJ/mol) for all sample.

As shown in Fig. 8, the adsorptions efficiencies of dye (reactive blue 19) adsorption for all samples were reached to the equilibrium state after approximately 3–10 min. The additional results of pseudo-kinetic and thermodynamic models are summarized in Tables 3 and 4, respectively. As expected, the adsorption kinetics of reactive dye using as-prepared adsorbents were fitted with the characteristic of pseudo-second order (based on $R^2>0.99$), suggesting to fast adsorption style. Herein, highest and lowest rate of iodine adsorption were in FS-Untreated (0.1237 min^{-1}) and FS-Treated by HNO_3 (0.0784 min^{-1}). Figure 9 presents the intra-particle diffusion result of dye (reactive blue 19) onto as-prepared adsorbent. As observed, this pattern was difference with the case of iodine diffusion since its single linearity were found in this plot. This should be attributed to

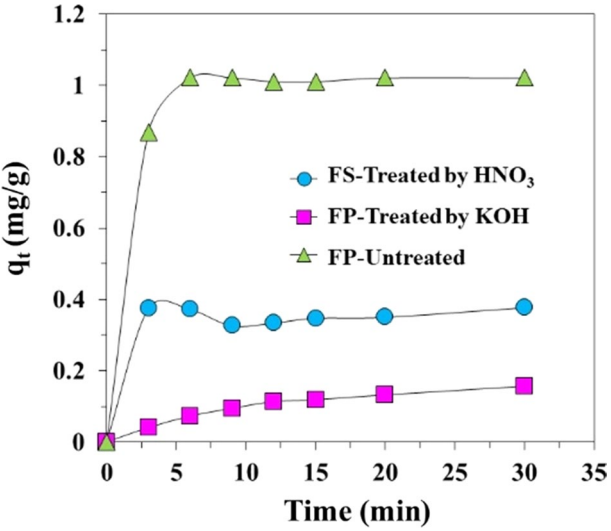

Fig. 8 Effect of contact time on removal efficiency of dye (reactive blue 19) using 25 mL of 20 ppm dye concentration, 3 to 30 min of contract times and 0.25 g of adsorbent

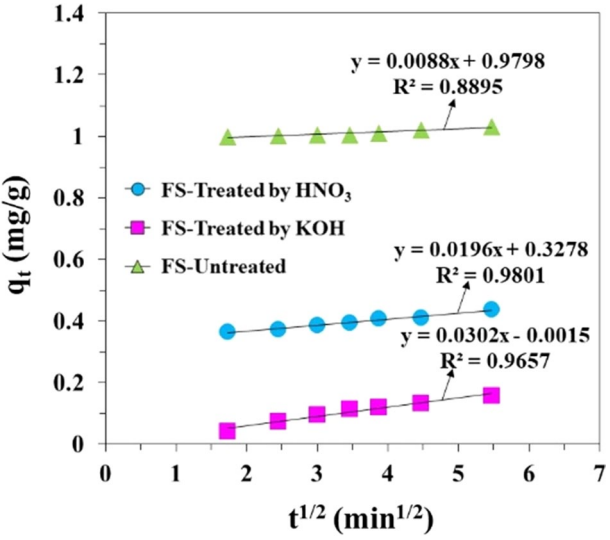

Fig. 9 Effect of intra-particle diffusion of dye (reactive blue 19) onto various adsorbents

different molecules size which the structure of reactive dye was much bigger than iodine. Meanwhile, their patterns of intra-particle diffusions were not also defined during rate-limiting step. For thermodynamic study of reactive blue 19, their adsorption behaviors were spontaneous physisorption with endothermic nature.

Adsorption capacity of synthetic wastewater

To approach more possibility for application in removal of industrial wastewater, the synthetic wastewater was carefully investigated by mixing of reactive blue 19, reactive yellow 3 and reactive red 22 at total concentration of 5 ppm. The initial and remaining concentrations of synthetic wastewater were defined by Cramer's method using matrix calculation process. For comparison, three chemical structures in each reactive dye are provided in Fig. 1. In addition, the surface areas of as-prepared adsorbents derived from methylene blue adsorption using Langmuir isotherm model with a maximum ability of monolayer adsorption are presented in Table 5. The range of surface area in FS sample was 18–20 m^2/g which was acceptable characteristic for lignocellulosic structure. The SEM images of adsorbents are presented in Fig. 10. As observed, a slight increasing of external surface area and porosity was found in FS-Treated by HNO_3 while the 3D surface of FS-Untreated and FS-Treated by KOH were quite smooth.

As shown in Fig. 11, the highest efficiency for removal of synthetic wastewater was obtained for CAC, which removal percentage for reactive blue 19, reactive yellow 3 and reactive red 22 were 97.35, 35.59 and 79.83%, respectively. This phenomenon should be described on much higher surface area (524.33 m^2/g) than other samples. In the case of FS-Carbon, higher efficiency for removal of synthetic wastewater was still found when compared with FS-Treated or FS-Untreated. However, these samples required high energy consumption for carbon preparation at high temperature and long reaction time, resulting in higher production cost, which was not suitable to be applied in practical process. In this work, low production cost with green adsorbent was required. Herein, even lower efficiency was found for FS when compared with CAC, but it was still better, considering on economic/eco-friendly points. However, high mount of FS was required when compared with a commercial one. Interestingly, for all samples, the reactive blue could be easier adsorbed than other reactive dyes, suggesting that the reactive blue 19 had molecular structure with smaller size than reactive yellow 3 and reactive red 22. Therefore, the effect of molecular size of reactive dye had high influence for adsorption ability, resulting from London force between carbon and reactive dye. For as-prepared FS, highest percentages for removals of reactive blue 19 (58.30%), yellow 3 (31.47%) and red 22 (18.91%) were achieved over FS-HNO_3 when compared with FS-Treated by KOH and FS-Untreated. Moreover, the reactive yellow was well adsorbed which was better than reactive red although molecular size of reactive red was smaller, probably due to the relation between mass force and/or charge force as well as

Table 5 Surface areas and maximum capacities of various adsorbents via methylene blue adsorption process

Adsorbent	Q_0 (mol/g)	R^2	Surface area (m^2/g)
FS-Treated by HNO_3	4.09×10^{-5}	0.9869	19.42
FS-Treated by KOH	3.89×10^{-5}	0.9825	18.47
FS-Untreated	3.94×10^{-5}	0.9847	18.71
FS-Carbon	4.53×10^{-5}	0.9850	21.51
CAC	1.81×10^{-3}	0.9980	524.33

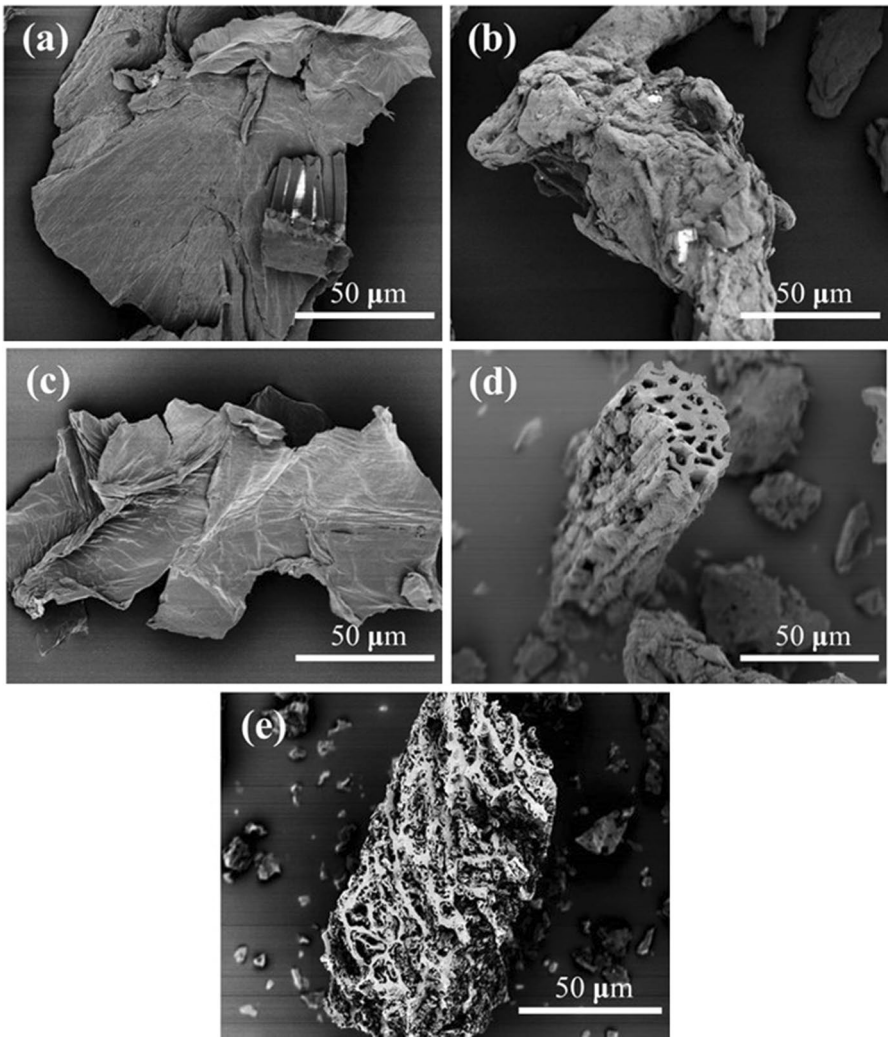

Fig. 10 SEM images of (**a**) FS-Untreated, (**b**) FS-Treated by HNO_3, (**c**) FS-Treated by KOH, (**d**) FS-Carbon and (**e**) CAC

polarity with surface area on theoretical adsorption [37]. This study provided high possibility to be truly applied in practical process.

Conclusions

In summary, FS was successfully prepared, modified and applied as the low-cost adsorbent for the removal of iodine and selected reactive dyes. The FS-Treated by HNO_3 was found suitable for the adsorption of reactive blue 19 (13.08 mg/g),

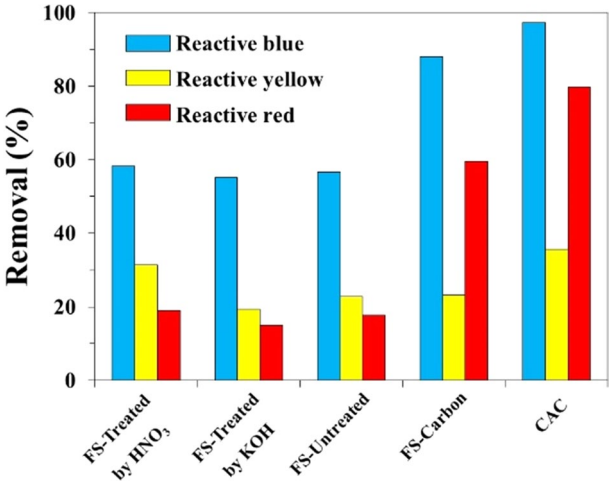

Fig. 11 Selective removal of synthetic wastewater over as-prepared adsorbents using 25 mL of 5 ppm synthetic wastewater concentration, 30 min of contract time and 0.5 g of adsorbent

while FP-Untreated exhibited a better result for the removal of iodine (340.00 mg/g). The adsorption equilibrium data of iodine and reactive blue 19 were well fitted with the Freundlich model, indicating the rapid/multilayer-physisorption behavior. Adsorption styles of iodine and reactive blue 19 for prepared adsorbents followed the pseudo-second-order model with no rate-limiting step. The thermodynamic adsorptions of iodine and reactive blue 19 were spontaneous physisorption with endothermic nature. The maximum adsorptions of reactive blue 19 (58.30%), yellow 3 (31.47%) and red 22 (18.91%) were derived over FS-Treated by HNO_3, while iodine was 87.3% using FS-Untreated. These results not only provide the adsorption behavior using FS but also offer promising such an alternative adsorbent for treatment of wastewater.

Supplementary Information The online version contains supplementary material available at https://doi.org/10.1007/s11164-022-04824-4.

Acknowledgements Authors would like to gratefully appreciate Department of Chemistry, Faculty of Science, Rangsit University, Thailand, for supporting the chemicals, equipment and instruments

Authors' contributions OT contributed to conceptualization, methodology and writing—original draft; HT contributed to conceptualization, methodology and writing—review and editing.

Funding Not applicable.

Declarations

Competing interests The authors declare no conflict of interest.

References

1. S. Banerjee, Res. Chem. Intermed. **44**, 4119 (2018)
2. P. Maneechakr, S. Karnjanakom, J. Environ. Chem. Eng. **9**, 106191 (2021)
3. Y.N. Kavil, Y.A. Shaban, S.S. Alelyani, R. Al-Farawati, M.I. Orif, M.A. Ghandourah, M. Schmidt, A.J. Turki, M. Zobidi, Res. Chem. Intermed. **46**, 755 (2020)
4. S.N. Jain, P.R. Gogate, J. Mol. Liq. **243**, 132 (2017)
5. P. Maneechakr, S. Karnjanakom, RSC Adv. **9**, 24074 (2019)
6. Q. Wang, C. Luo, Z. Lai, S. Chen, D. He, J. Mu, Bioresour. Technol. **357**, 127363 (2022)
7. S. Dash, H. Chaudhuri, R. Gupta, U.G. Nair, J. Environ. Chem. Eng. **6**, 5897 (2018)
8. C. Li, H. Xia, L. Zhang, J. Peng, S. Cheng, J. Shu, S. Zhang, Res. Chem. Intermed. **44**, 2231 (2018)
9. F. Mbarki, T. Selmi, A. Kesraoui, M. Seffen, Ind. Crops Prod. **178**, 114546 (2022)
10. Z. Ma, Y. Han, J. Qi, Z. Qu, X. Wang, Ind. Crops Prod. **169**, 113649 (2021)
11. J. Zhou, S. Hao, L. Gao, Y. Zhang, Ann. Nucl. Energy **72**, 237 (2014)
12. P. Maneechakr, S. Karnjanakom, Res. Chem. Intermed. **45**, 4583 (2019)
13. S.N. Jain, P.R. Gogate, J. Environ. Manage. **210**, 226 (2018)
14. S. Karnjanakom, Y. Ma, G. Guan, P. Phanthong, X. Hao, X. Du, C. Samart, A. Abudula, Electrochim. Acta **139**, 36 (2014)
15. H. Haroon, T. Ashfaq, S.M.H. Gardazi, T.A. Sherazi, M. Ali, N. Rashid, M. Bilal, Korean J. Chem. Eng. **33**, 2898 (2016)
16. P. Ashokan, M. Asaithambi, V. Sivakumar, P. Sivakumar, Groundw. Sustain. Dev. **15**, 100671 (2021)
17. A. Khasri, O.S. Bello, M.A. Ahmad, Res. Chem. Intermed. **44**, 5737 (2018)
18. J.A. Shah, T.A. Butt, C.R. Mirza, A.J. Shaikh, M.S. Khan, M. Arshad, N. Riaz, H. Haroon, S.M.H. Gardazi, K. Yaqoob, M. Bilal, Molecules **25**, 2118 (2020)
19. M. Konneh, S.M. Wandera, S.I. Murunga, J.M. Raude, Heliyon **7**, e08458 (2021)
20. H. Babas, M. Khachani, I. Warad, S. Ajebli, A. Guessous, A. Guenbour, Z. Safi, A. Berisha, A. Bellaouchou, Z. Abdelkader, G. Kaichouh, J. Mol. Liq. **356**, 119019 (2022)
21. S. Charola, R. Yadav, P. Das, S. Maiti, Sustainable. Environ. Res. **28**, 298–308 (2018)
22. M. Bilal, J.A. Shah, T. Ashfaq, S.M.H. Gardazi, A.A. Tahir, A. Pervez, H. Haroon, Q. Mahmood, J. Hazard. Mater. **263**, 322 (2013)
23. H. Haroon, S.M.H. Gardazi, T.A. Butt, A. Pervez, Q. Mahmood, M. Bilal, Pol. J. Chem. Technol. **19**, 6 (2017)
24. U. Özdemir, B. Özbay, I. Özbay, S. Veli, Ecotoxicol. Environ. Saf. **107**, 229 (2014)
25. P. Gao, G. Li, F. Yang, X.N. Lv, H. Fan, L. Meng, X.Q. Yu, Ind. Crops Prod. **48**, 61 (2013)
26. R. Zuluaga, J.L. Putaux, J. Cruz, J. Vélez, I. Mondragon, P. Gañán, Carbohydr. Polym. **76**, 51 (2009)
27. M. Moniruzzaman, J.M. Bellerby, M.A. Bohn, Polym. Degrad. Stab. **102**, 49 (2014)
28. S. Karnjanakom, P. Maneechakr, J. Mol. Struct. **1186**, 80 (2019)
29. H.K. Yağmur, I. Kaya, J. Mol. Struct. **1232**, 130071 (2021)
30. P. Maneechakr, P. Chaturatphattha, S. Karnjanakom, Res. Chem. Intermed. **44**, 7135 (2018)
31. J. Pérez-Calderón, M.V. Santos, N. Zaritzky, React. Funct. Polym. **155**, 104699 (2020)
32. P. Moeini, A. Bagher, Res. Chem. Intermed. **46**, 5547 (2020)
33. D. Pandey, A. Daverey, K. Dutta, V.K. Yata, K. Arunachalam, Technol. Innovation **25**, 102200 (2022)
34. Z. Wang, S.B. Kang, S.W. Won, Colloids Surf. A **647**, 128983 (2022)
35. P. Maneechakr, S. Karnjanakom, J. Chem. Thermodyn. **106**, 104 (2017)
36. Y. Guo, Z. Wang, X. Zhou, R. Bai, Res. Chem. Intermed. **43**, 2273 (2017)
37. M. Ghaedi, N. Mosallanejad, J. Ind. Eng. Chem. **20**, 1085 (2014)